

Article

# Design of a Novel Linear Shaped Charge and Factors Influencing its Penetration Performance

Xi Cheng <sup>1</sup>, Guangyan Huang <sup>1,\*</sup>, Chunmei Liu <sup>2</sup> and Shunshan Feng <sup>1</sup>

<sup>1</sup> State Key Laboratory of Explosion Science and Technology, Beijing Institute of Technology, Beijing 100081, China; bitchengxi@bit.edu.cn (X.C.); ssfeng@bit.edu.cn (S.F.)

<sup>2</sup> First Research Institute of Ministry of Public Security of PRC, Beijing 100044, China; liuchunmei0127@163.com

\* Correspondence: huanggy@bit.edu.cn; Tel.: +86-010-6891-5532

Received: 9 September 2018; Accepted: 8 October 2018; Published: 10 October 2018



**Featured Application:** This work provides a new type of linear shaped charge, and it is meaningful for the structural design of the novel linear shaped charge.

**Abstract:** In this paper, a novel linear shaped charge (LSC), called a bi-apex-angle linear shaped charge (BLSC), has been designed to investigate the improvement of penetration performance. Compared with a traditional single-apex-angle LSC, a BLSC, which consists of a small-apex-angle liner and a large-apex-angle liner, has been investigated by depth-of-penetration (DOP) test. The results show that the penetration depth of BLSC is 29.72% better than that of an ordinary LSC. An Eulerian method is applied to simulate the entire process of jet formation, as well as penetration on a #45 steel target. The effectiveness of the Eulerian model is demonstrated by the good agreement of the computational results with experimental observations. Furthermore, the numerical simulation is developed to investigate the influence of liner thickness, explosive type, combination of small and large apex angle, ratio of small to all apex angle liner, and standoff distance on the penetration performance of BLSCs. The suggested work and results can provide a guide and reference for the structural design of BLSC.

**Keywords:** shaped charge; Bi-apex-angle liner; influence factor; penetration performance

## 1. Introduction

In some emergencies, such as suspect capture, emergency rescue, and fire rescue, the first question is how to quickly open an emergency passage. One of the most effective ways is using a metal jet formed by a linear shaped charge (LSC), which can break up obstacles and reduce collateral damage.

Since the pioneering work of G. Birkhoff, the steady state theory of Birkhoff and the unsteady state theory of PER (Pugh, Eichelberger, and Rosstoker) have been widely used in studies of shaped charges. Most of the researches in this field are focused on conical shaped charges (CSCs) and there have been few publications about LSCs [1,2]. Zeng [3] proposed an unsteady theory of jet formation for end-initiated LSCs, and confirmed that the theory agreed well with experimental results in the case of a charge with constant thickness. With the development of numerical simulation technology, the mechanism of LSC jet formation has been further analyzed and researched. Lim established a steady-state analytical equation of motion of a LSC's liner based on the modification of the original Birkhoff theory [4] and showed that compared with numerical simulation results created with Autodyn software, this analytical equation exhibited favorable results in a limited range. Lim also proposed a theoretical model to predict the behavior of an explosively driven flyer, and calculated the jet tip velocity based on the formation of an arc in the liner. Some researchers studied the characteristics of the

liner collapse line using a typical jet flight pattern of LSC [5–9]. For the simulation method, smoothed particle hydrodynamics (SPH) was used to investigate the formation process of a linear-shaped charge jet [10–12]. Miyoshi conducted a standoff test of a LSC that provided significant information about determining the optimal standoff distance and allowed the design of effective cutting plans for use with LSCs [13,14]. Vinko Škrlec experimentally determined the effects of a mass of explosive, liner material and standoff distance on the penetration depth of the LSCs [15,16].

The shape of a shaped charge liner has great influence on the formation of metal jet and its penetration performance into a target. The researchers mainly focused on LSCs with a single-apex-angle liner. This paper describes an experiment using bi-apex-angle linear shaped charges (BLSCs) for effective penetration. A typical BLSC is shown in Figure 1. The greatest difference distinguishing a BLSC from the traditional LSC is a small-apex-angle liner that is added in an ordinary LSC liner. In this paper, the penetration performance of a BLSC is tested by the depth-of-penetration (DOP) test, and the results show that its penetration depth is 29.72% better than that of an ordinary LSC. The penetration performance of the BLSC and LSC is then investigated by Autodyn-2D. Based on the validated numerical approach and models, we comprehensively discussed the influences of liner thickness, explosive type, a combination of small and large apex angles, and a ratio of small to all apex angle liners on the penetration performance of BLSCs. The present study provides a guidance and reference for the structural design of a BLSC.

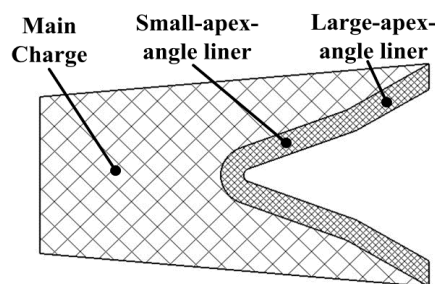


Figure 1. Schematic of a bi-apex-angle linear shaped charge (BLSC).

## 2. Experiment

The schematic of the BLSC is shown in Figure 2, where  $d_1$ ,  $2a_1$ ,  $d_2$ ,  $2a_2$ ,  $\theta$ ,  $\delta$ , and  $H$  are the width of the small-apex-angle liner, the small apex angle, the width of large-apex-angle liner, the large apex angle, the charge slope angle, the liner thickness, and the charge height, respectively.

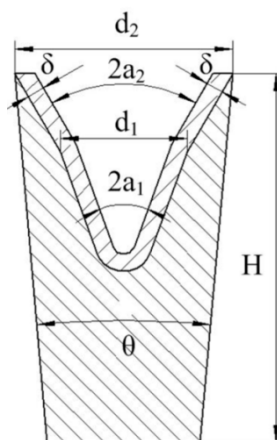


Figure 2. Schematic of the BLSC.

### 2.1. Preparation of the Bi-Apex-Angle Liner

A bi-apex-angle liner is distinguished by a small-apex-angle liner that is added to an ordinary liner. A typical bi-apex-angle liner is shown in Figure 3. Table 1 shows the related parameters of the BLSC liner.

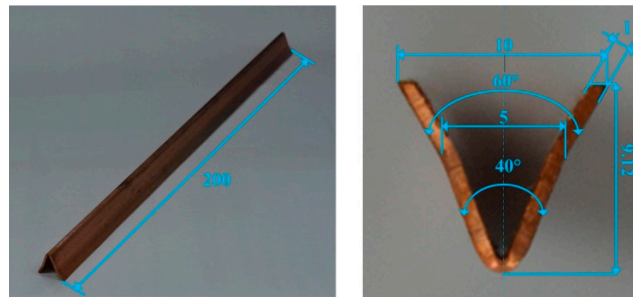


Figure 3. Bi-apex-angle liner used in the experiment.

Table 1. Parameters of the BLSC liner.

$d_1$	$d_2$	$\theta$	$2a_1$	$2a_2$
5 mm	10 mm	$10^\circ$	$40^\circ$	$60^\circ$

### 2.2. Experimental Bi-Apex-Angle Linear Shaped Charge

The BLSC used in the experiment consisted of the main charge, a bi-apex-angle liner, and a shell, as shown in Figure 4. The main charge was an 8701 explosive, which was placed in a press mold and subjected to a pressure load at room temperature. The height of the main charge (H) was 17 mm. Because of the design of bi-apex-angle liner, the mass of the BLSC main charge decreased by 1.1% compared to an LSC charge under the same density and the height (H). The bi-apex-angle liner was made from a 1.0 mm T2 copper plank. The shell was made from polymeric methyl methacrylate (PMMA). It provided a 10 mm standoff distance (the same as the width), and the influences of the shell were neglected.

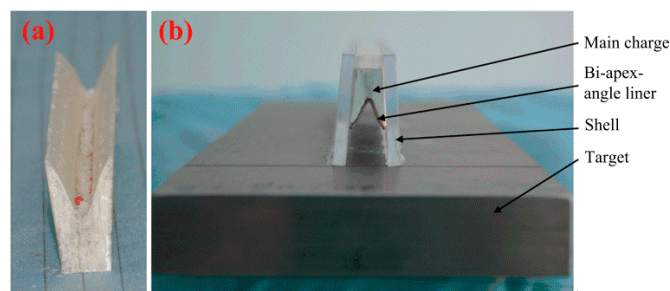


Figure 4. (a) Main charge; (b) BLSC and target.

### 2.3. Depth of Penetration (DOP) Experiment

An experiment using the DOP method was conducted to investigate the penetration performance of a BLSC against that of an ordinary LSC. The LSC had a constant  $60^\circ$  apex-angle liner, and the other parameters were the same as the experimental BLSC. The experimental setup is shown in Figure 5. These shaped charges were centrally initiated through a #8 electric detonator at one end. To measure the penetration depth is important when studying the difference in penetration performance between the LSC and BLSC. A 45 steel target was set to measure the penetration capability of the two shaped charges. It had a density of  $7.85 \text{ g/cm}^3$  and measured 300 mm (l)  $\times$  100 mm (w)  $\times$  20 mm (h).

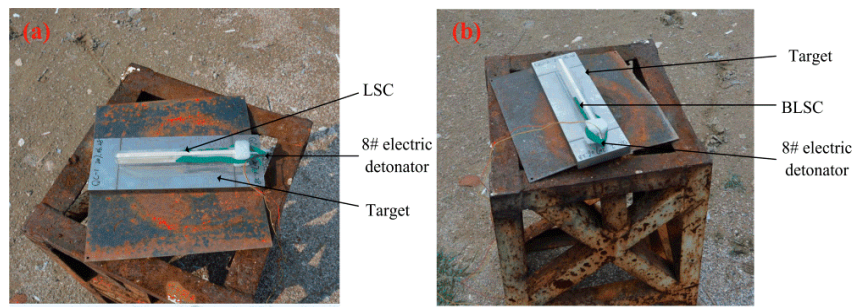


Figure 5. (a) Main charge; (b) BLSC and target.

### 3. Numerical Simulation

#### 3.1. Numerical Algorithms

The numerical simulation is carried out in software Autodyn. This software has been widely used to analyze the nonlinear dynamic impacts and explosions. It allows the application of different algorithms such as Euler, Lagrangian, Arbitrary Lagrangian Euler (ALE), and SPH to solve the fluid–structure problems [17]. In this current work, because LSCs are much larger in the longitudinal direction than in other two directions, they can be modeled as a plane strain problem in a two-dimensional space [4,10,11,14] and numerically simulated using the explicit nonlinear dynamic analysis software ANSYS Autodyn-2D version 17.2 (ANSYS Inc.: Canonsburg, PA, USA, 2016). By using the multi-material Eulerian algorithm, the whole process including the jet formation, flight of jet, slug and wing, and the impact on the steel target was reproduced.

#### 3.2. Establishment of the Simulation Model

A numerical analysis model is simplified to two-dimensional plane-symmetric geometries for efficient calculation, as shown in Figure 6. The geometrical parameter in the simulation model was the same as the one in the DOP test. The charge was 8701 and it was centrally initiated through a simple detonator at the bottom.

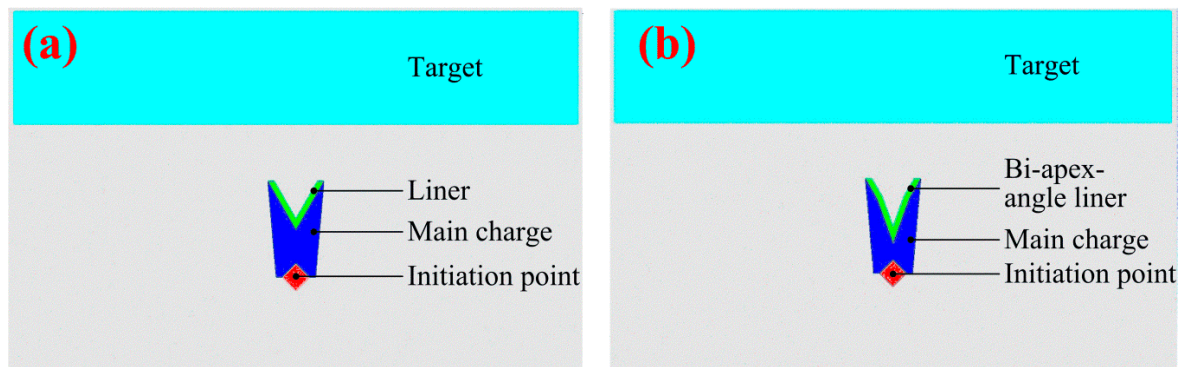


Figure 6. Numerical model of shaped charges: (a) LSC; (b) BLSC.

In the calculation, the 8701 explosive is used. The equation of state (EOS) of the 8701 explosive is Jones-Wilkins-LEE (JWL). The liner material is made of T2 copper. The mechanical model of CU-OFHC in Autodyn is regarded as T2 copper. The EOS and strength of T2 copper were Shock and Streinberg Gruinan, respectively. The material of the steel target was #45 steel; its dynamic response behavior under the action of the detonation wave can be described using the Johnson–Cook (J–C) material model. An air grid covered the penetrator flying range. The type of air model was taken from Autodyn, and the Int Energy of air is  $2.068 \times 10^5$ . The parameters of all material models used in the calculation are listed in Table 2 [18,19].

**Table 2.** Parameters of material model.

8701	Density (g/cm <sup>3</sup> )	A (kPa)	B (kPa)	R1	R2	W	C–J Detonation velocity (m/s)	C–J Energy/unit volume (kJ/m <sup>3</sup> )	C–J Pressure (kPa)	
	1.713	$5.242 \times 10^8$	$7.768 \times 10^6$	4.2	1.1	0.34	7980	$8.499 \times 10^6$	$2.86 \times 10^7$	
#45 Steel	Density (g/cm <sup>3</sup> )	Shear modulus (kPa)	Yield stress A (kPa)	Hardening constant B (kPa)	Hardening exponent	Strain rate constant	Thermal softening exponent	Melting temperature Tm (K)	Ref. strain rate (/s)	Strain rate correction
	7.83	$7.59 \times 10^7$	$3.5 \times 10^5$	$3.2 \times 10^5$	0.28	0.064	1.06	$1.793 \times 10^3$	1.0	1st Order
CU-OFHC	Density (g/cm <sup>3</sup> )	Shear modulus (kPa)	Yield stress A (kPa)	Maximum Yield stress (kPa)	Hardening constant	Hardening Exponent	Derivative dG/dP	Derivative dG/dT (kPa/K)	Derivative dY/dp	Melting Temperature (K)
	8.93	$4.77 \times 10^7$	$1.2 \times 10^5$	$6.4 \times 10^5$	36	0.45	1.35	$-1.798 \times 10^4$	$3.39 \times 10^{-3}$	$1.79 \times 10^3$
Air	Density (g/cm <sup>3</sup> )	Gamma	Adiabatic constant	Pressure shift (kPa)	Reference Temperature (K)	Specific Heat (J/kgK)	Thermal Conductivity (J/mKs)	Int Energy		
	0.001225	1.4	0	0	288.200012	717.599976	0	$2.068 \times 10^5$		

### 4. Results

#### 4.1. Experimental Results

The LSC and BLSC exhibited excellent damage effects, as illustrated in Figure 7.

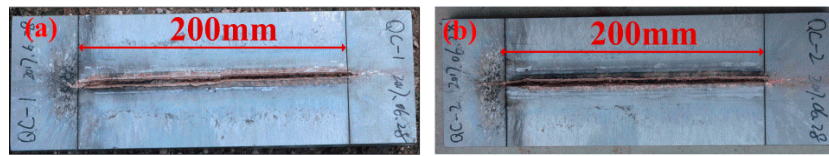


Figure 7. Experimental results of shaped charges: (a) LSC; (b) BLSC.

To investigate the penetration depths of the LSC and BLSC, the targets were cut vertically along penetration cracks. Every target was divided into eight parts. Figure 8 provides detailed data about the penetration depth on each side of every part.

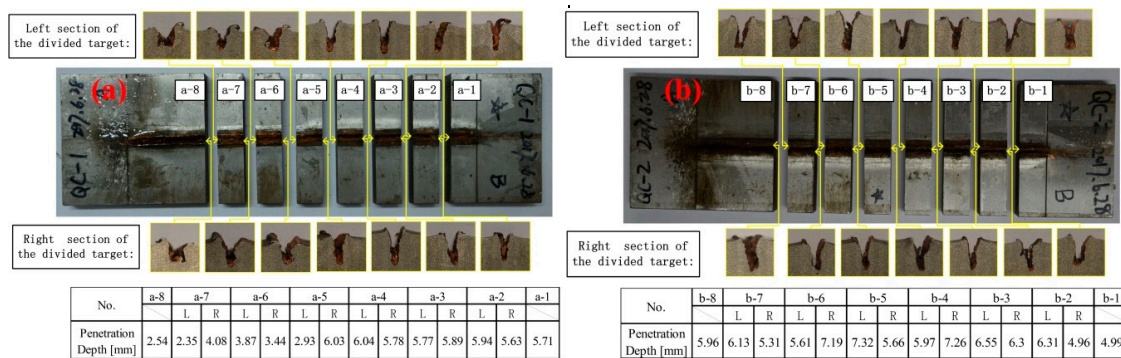


Figure 8. Penetration depth of shaped charges: (a) LSC; (b) BLSC.

Where  $P_e$  is the penetration depth of experimental test. It is shown as:

$$P_e = \frac{\sum_{i=1}^n P_i}{n} \tag{1}$$

#### 4.2. Numerical Simulation Results

Typical jet formation and penetration processes of an LSC and BLSC are shown in Figure 9. After the explosion, the copper liner elements gradually moved to the symmetry plane and collapsed under the action of the detonation wave. When the copper liner elements arrived at the collision point, the velocity of the outer liner elements was lower than that of the inner liner elements; hence, the outer liner elements moved to the left of the collision point and formed a slug. At the same time, the inner liner elements moved to the right of the collision point and formed a jet. The remaining copper liner elements, which did not arrive at the collision point, forming an alae. Therefore, the colliding liner elements were divided into three parts: jet, slug, and alae.

The penetration depths, as well as the DOP test results for the LSC and BLSC, are graphically illustrated in Figure 8, and Figure 9 shows the typical numerical results of jet formation and penetration processes described by Autodyn. Furthermore, Table 3 shows the good agreement between the experiment and numerical simulation outputs. These indicate that the adopted numerical constitutive models and corresponding parameters are able to give reliable predictions of penetration performance of LSCs and BLSCs.

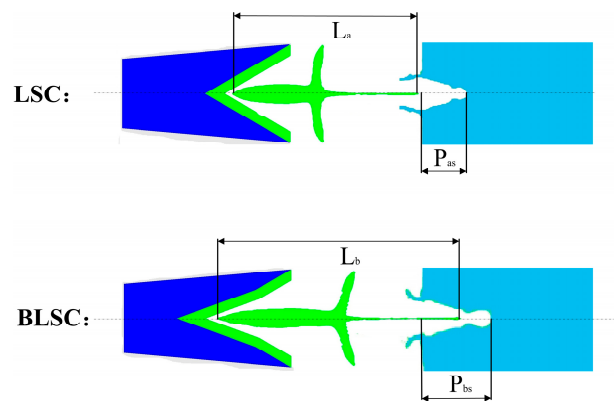


Figure 9. Numerical simulation of jet formation and penetration processes.

Table 3. Parameters of material model.

Type	Ps (mm)	Pe (mm)	Difference (mm)	Percentage Error
LSC	4.75	4.71	0.04	0.85%
BLSC	6.00	6.11	0.11	1.80%

### 5. Parametric Influences on Penetration Performance

Based on our results, as well as the verified numerical constitutive models and the corresponding parameters, the influences of liner thickness, explosive type, combination of small and large apex angle, ratio of small to all apex angle liner, and standoff distance on the penetration performance of BLSCs are further discussed.

#### 5.1. Liner Thickness

Based on the presented numerical simulation result of the BLSC, another four sets of penetration scenarios with the liner thickness ( $\delta$ ) of 0.4 mm, 0.6 mm, 0.8 mm, and 1.2 mm are further complemented. The other parameters, such as  $d_1$ ,  $2a_1$ ,  $d_2$ ,  $2a_2$ , and  $\theta$ , are shown in Table 1.

Figure 10 shows the velocity distribution of jet with different liner thicknesses before penetration. Figure 11 presents the relationship between the liner thickness and penetration depth. It is obvious that the jet velocity is getting higher and the total length of jet and slug is increasing rapidly with the decrease of liner thickness. Thus, the BLSC with a 0.4 mm liner has a better penetration performance than others. But, taking into account the processing technic and assembling of a BLSC, the 0.6 mm liner is recommended in this paper.

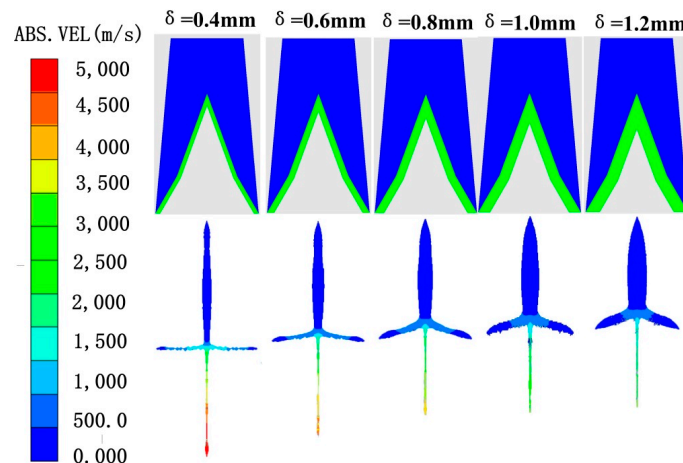


Figure 10. Velocity distribution of different liner thickness.

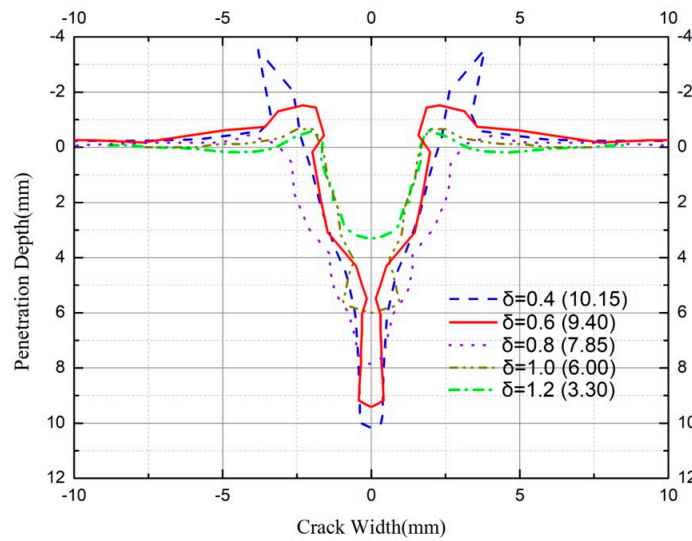


Figure 11. Penetration depth of BLSCs with different liner thickness.

5.2. Explosive Type

Based on the penetration performance of the BLSC with 0.6 mm liner, another four sets of DOP tests on steel targets with the explosives of COMP B, C-4, TNT, and LX-19 were further simulated. Table 4 shows the corresponding parameters of these explosives [20]. Figure 12 shows the velocity distribution with the above five different explosives before penetration. Figure 13 further illustrates the sectional penetration cracks, and the values of penetration depths are shown in the parentheses.

Table 4. Parameters of four explosives.

Parameters	COMP B	C-4	TNT	LX-19
Density(g/cm <sup>3</sup> )	1.717	1.601	1.630	1.942
A (kPa)	$5.24 \times 10^8$	$6.10 \times 10^8$	$3.71 \times 10^8$	$1.64 \times 10^9$
B (kPa)	$7.68 \times 10^6$	$1.30 \times 10^7$	$3.21 \times 10^6$	$1.86 \times 10^7$
R1	4.2	4.5	4.15	6.5
R2	1.1	1.4	0.95	2.7
W	0.34	0.25	0.3	0.55
C-J Detonation velocity (m/s)	7,980	8,190	6,930	9,208
C-J Energy/unit volume (kJ/m <sup>3</sup> )	$8.50 \times 10^6$	$9.00 \times 10^6$	$4.30 \times 10^6$	$1.15 \times 10^7$
C form alae J Pressure (kPa)	$2.95 \times 10^7$	$2.80 \times 10^7$	$2.10 \times 10^7$	$4.30 \times 10^7$

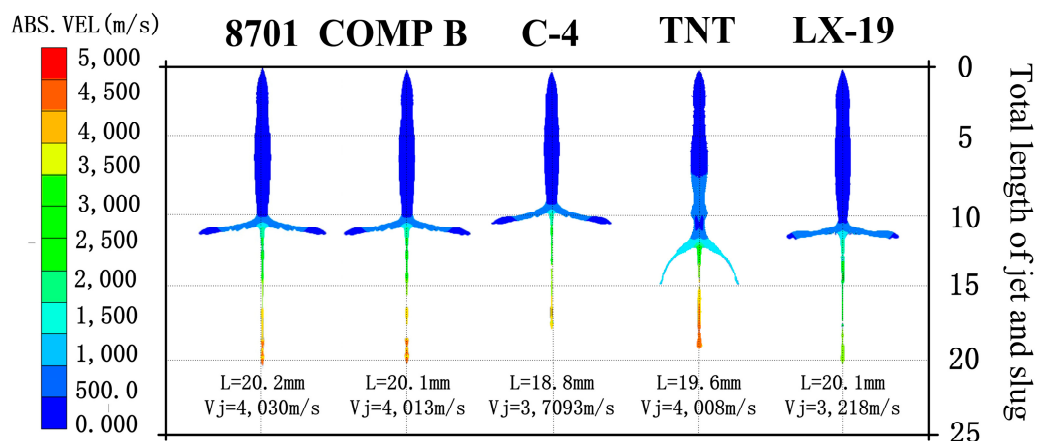


Figure 12. Velocity distribution of different explosives.

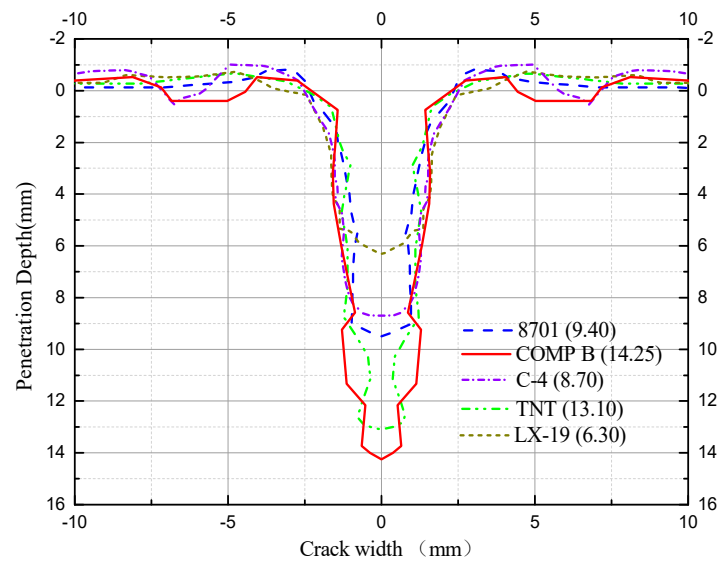


Figure 13. Penetration depth of BLSCs with different explosives.

According to these figures, it should be noted that the penetration depth is a result of a multitude of factors such as jet tip velocity, jet length, velocity distribution and so on. The jet tip velocities of BLSCs with 8701, COMP B, and TNT are much higher than those with C-4 and LX-19. The jet/slug lengths of BLSCs with 8701, COMP B, and TNT are also longer than those of the others. As shown in Figure 13, the penetration depth of BLSC with COMP B is the deepest, followed in turn by that of BLSCs with TNT, 8701, C-4, and LX-19, which is the smallest. Although the jet/slug length of BLSC with LX-19 is not the shortest, it has the minimal penetration depth, indicating that the velocity has greater influence on the penetration depth of BLSC than jet/slug length.

### 5.3. Combinations of Small and Large Apex Angles

The influence of small and large apex angle is further discussed in this part. Figure 14 shows the numerical results of BLSC with 0.6 mm thick liner, COMP B as the explosive and different combinations of small apex angle ( $2\alpha_1 = 30^\circ, 40^\circ, 50^\circ$  and  $60^\circ$ , respectively) and large apex angle ( $2\alpha_2 = 60^\circ, 80^\circ$  and  $100^\circ$ , respectively).

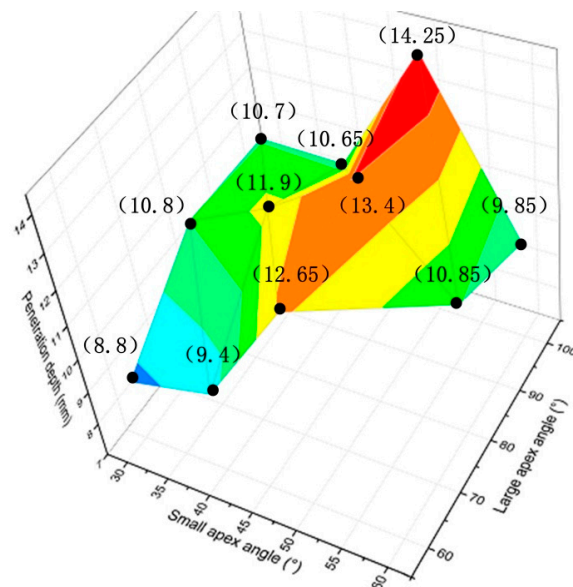


Figure 14. Penetration depths of different combinations of small and large apex angles.

It shows that, (i) with the small apex angle increasing, the penetration depth shows a trend of increase before a decrease; and (ii) with the large apex angle increasing, the penetration depth shows a trend of increase before decreasing as well. The reason is that when the small apex angle starts increasing, the jet velocity is getting slower but the jet mass is becoming bigger. Therefore, the penetration depth becomes deeper. With the small apex angle further increasing, the jet velocity drops dramatically and the penetration depth decreases. The part liner with large apex angle mainly forms the wing and the slug. Therefore, when the large apex angle starts increasing, the part that forms effective slug penetrating into a steel target speeds up, resulting in a deeper penetration depth. With the large apex angle further increasing, the mass of effective slug decreases, resulting in a smaller penetration depth. It should be noted that to make the charge height H remain constant, the differences of the explosive mass varies from 30.4 g/200 mm to 40.4 g/200 mm and this cannot be ignored.

#### 5.4. Ratio of Small to All Apex Angle Liners

The effect of liners with different ratios of small to all apex angle ( $n = d_1/d_2$ ) on penetration depth is further explored using BLSCs with 0.6 mm thick liner, COMP B as the explosive, small apex angle of  $50^\circ$ , large apex angle of  $100^\circ$ , and  $n = 0.3, 0.4, 0.5, 0.6,$  and  $0.7$ , respectively. Figure 15 represents the penetration performance of BLSCs with different values of  $n$ .

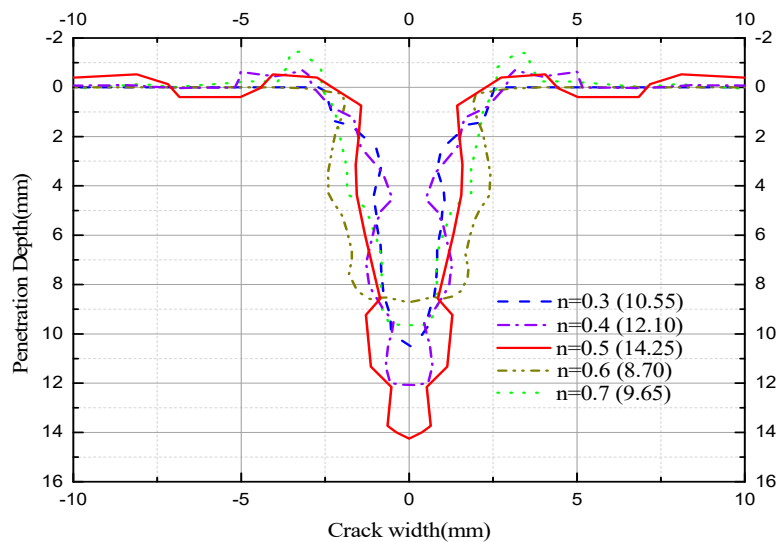


Figure 15. Penetration depth of BLSCs with different ratios of small to all apex angles.

It should be noted that the mass of explosive changes as the  $n$  charges. Taking a 200 mm long BLSC as an example, the mass of explosive is 41.32 g, 40.55 g, 39.54 g, 38.31 g and 36.86 g when  $n = 0.3, 0.4, 0.5, 0.6,$  and  $0.7$ , respectively. Figure 15 illustrates the sectional penetration cracks and the penetration depths are shown in the parentheses. Taking the energy efficiency and the penetration performance into account, a BLSC with  $n = 0.5$  may be the best.

#### 5.5. Standoff Distance

The standoff distance (S) is the distance between a BLSC and a target. It is also an important factor that influences the penetration performance of BLSCs. The efficiency of the BLSC is increased to a certain standoff distance, which is called the optimal standoff distance. With a 0.6 mm thick liner, COMP B,  $2a_1 = 50^\circ$  and  $2a_2 = 100^\circ$ , and  $n = 0.5$ , the penetration performance of BLSCs is simulated with different S (S = 4, 6, 8, 10, and 12 mm, respectively.)

As can be seen from Figure 16, for the tested construction of the BLSCs, the greatest penetration depth is about 14.25 mm, and this is achieved at the standoff distance of 10 mm. It should be noted that there are two peaks on the penetration depth-standoff distance curves. However, there is not yet a

full understanding about the formation of these two peaks. The possible reason is that the velocity gradient in the jet formed by the BLSCs is different from the one that is formed by the ordinary LSCs, and this leads to a different distribution pattern of penetration performance.

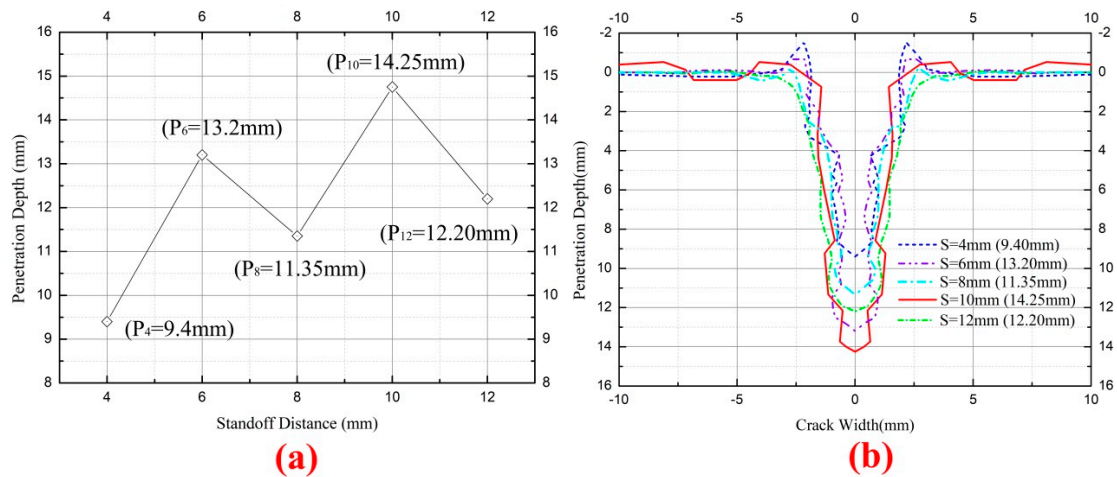


**Figure 16.** Penetration depth of BLSCs with different standoff distance: (a) Penetration depth of various standoff distance; (b) Sectional penetration crack.

## 6. Conclusions

The penetration performance of a novel linear shaped charge, BLSC, is discussed in this paper. Compared with the ordinary LSC with a constant  $60^\circ$  apex-angle liner, the BLSC, which contains a  $40^\circ$  small-apex-angle liner and a  $60^\circ$  large-apex-angle liner, greatly improves the efficiency of the main charge energy. With a 1.0 mm liner thickness, 8701 explosive, and 10 mm standoff distance, the DOP tests show that the penetration performance of the BLSC is 29.72% better than that of an ordinary LSC for a #45 steel target.

The results from the numerical simulations in a multi-material Eulerian algorithm of penetration performance are all in good agreement with the DOP tests, thus verifying the feasibility and effectiveness of the presented Eulerian model.

For the BLSC with 0.6 mm thick liner, COMP B as an explosive, small apex angle of  $50^\circ$  and  $100^\circ$ , respectively,  $n = 0.5$ , and  $S = 10$  mm is recommended to attain the best penetration performance on a #45 steel target. The greatest penetration depth is about 14.25 mm.

All the results provide a guide and reference for the structural design of BLSC.

**Author Contributions:** X.C. wrote the article; G.H. and S.F. contributed to scientific discussions; C.L. proposed the original idea.

**Funding:** This research was funded by [the National Natural Science Foundation of China] grant number [11772059], and [the National Key Research and Development Program of China] grant number [2017yfc0822300].

**Conflicts of Interest:** The authors declare no conflict of interest.

## References

1. Meryl, M.; Tom, K. Performance analysis of linear shaped charge for aerospace applications. In Proceedings of the 41st AIAA/ASME/SAE/ASEE Joint Propulsion Conference & Exhibit, Tucson, AZ, USA, 10–13 July 2005.
2. Dave, N.; Meryl, M. Historical development of linear shaped charge. In Proceedings of the 43rd AIAA/ASME/SAE/ASEE Joint Propulsion Conference & Exhibit, Cincinnati, OH, USA, 8–11 July 2007.
3. Zeng, X.; Xue, H. A theory study on linear shaped charges. *Explos. Shock Waves* **1988**, *2*, 97–105.
4. Lim, S. Steady state equation of motion of a linear shaped charges liner. *Int. J. Impact Eng.* **2012**, *10*, 10–16. [[CrossRef](#)]

5. Lim, S. Steady state analytical equation of motion of linear shaped charges jet based on the modification of Birkhoff theory. *Appl. Sci.* **2012**, *2*, 35–41. [[CrossRef](#)]
6. Lim, S. Jet velocity profile of linear shaped charges based on an arced liner collapse. *J. Energ. Mater.* **2013**, *31*, 239–250. [[CrossRef](#)]
7. Lim, S. Acceleration profile of a flat flyer driven by detonation isentrope. *Propellants Explos. Pyrotech.* **2013**, *38*, 410–418. [[CrossRef](#)]
8. Lim, S. Jet flight patterns of linear shaped charges. *J. Energ. Mater.* **2016**, *34*, 14–25. [[CrossRef](#)]
9. Lim, S. Liner Collapse Line of Linear Shaped Charges. *J. Energ. Mater.* **2016**, *35*, 125–135. [[CrossRef](#)]
10. Gang, Y.; Xu, H.; De'an, H. Computer simulation of two-dimensional linear-shaped charge jet using smoothed particle hydrodynamics. *Eng. Comput.* **2011**, *28*, 58–75. [[CrossRef](#)]
11. Feng, D.L.; Liu, M.B.; Li, H.Q.; Liu, G.R. Smoothed particle hydrodynamics modeling of linear shaped charge with jet formation and penetration effects. *Comput. Fluids* **2013**, *86*, 77–85. [[CrossRef](#)]
12. BaêtaNeves, A.P.; Ferreira, A. Shaped charge simulation using SPH in cylindrical coordinates. *Eng. Comput.* **2015**, *32*, 370–386. [[CrossRef](#)]
13. Miyoshi, H.; Ohba, H.; Inoue, T.; Kitamura, H.; Inoue, T.; Hiroe, T. Evaluation of Penetration Performance for Linear Shaped Charges. *Jpn. Soc. Aeronaut. Space Sci.* **2005**, *53*, 231–236.
14. Miyoshi, H.; Ohba, H.; Kitamura, H.; Inoue, T.; Hiroe, T. Improvement of penetration performance of linear shaped charges. *Proj. Impact* **2014**, *75*, 87–96.
15. Bohanek, V.; Dobrilovic, M.; Škrlec, V. Jet velocity of linear shaped charges. *Rud. Geol. Naft. Zb.* **2012**, *25*, 73–80.
16. Bohanek, V.; Dobrilovic, M.; Škrlec, V. The efficiency of linear shaped charges. *Teh. Vjesn.* **2014**, *21*, 525–531.
17. Li, W.; Huang, G.; Feng, S. Effect of eccentric edge initiation on the fragment velocity distribution of a cylindrical casing filled with charge. *Int. J. Impact Eng.* **2015**, *80*, 107–115. [[CrossRef](#)]
18. Li, W.; Wang, X.; Li, W. The effect of annular multi-point initiation on the formation and penetration of an explosively formed penetrator. *Int. J. Impact Eng.* **2010**, *37*, 414–424. [[CrossRef](#)]
19. ANSYS/Autodyn-2D and 3D; Version 17.2; User Documentation; ANSYS Inc.: Canonsburg, PA, USA, 2016.
20. Hu, F.; Wu, H.; Fang, Q.; Liu, J.; Liang, B.; Kong, X. Impact performance of explosively formed projectile (EFP) into concrete targets. *Int. J. Impact Eng.* **2017**, *109*, 150–166. [[CrossRef](#)]



© 2018 by the authors. Licensee MDPI, Basel, Switzerland. This article is an open access article distributed under the terms and conditions of the Creative Commons Attribution (CC BY) license (<http://creativecommons.org/licenses/by/4.0/>).